Investigating the Effect of Size and Site of Implantation on Tumour Vascular Morphology and Function Using Combined Carbogen USPIO (CUSPIO) Imaging

J. S. Burrell[1], J. Halliday[2], S. Walker-Samuel[3], J. C. Waterton[2], J. Boult[1], Y. Jamin[1], L. C. Baker[1], and S. P. Robinson[1]
[1]The Institute of Cancer Research, Sutton, Surrey, United Kingdom, [2]AstraZeneca, Manchester, United Kingdom, [3]UCL, London, United Kingdom

Introduction: The combined carbogen USPIO imaging protocol (CUSPIO) combines two MRI susceptibility contrast mechanisms: intrinsic susceptibility contrast MRI and contrast enhanced susceptibility MRI with ultra small super paramagnetic iron oxide (USPIO) particles [1]. R_2* ($1/T_2$*) slows with high oxygen-content gas breathing, which decreases the ratio of deoxyhaemoglobin (paramagnetic) to oxyhaemoglobin (diamagnetic) in blood. The resulting change in R_2*, $\Delta R_2^*_{carbogen}$, reflects changes in oxygenation and the haemodynamic response in functional vasculature. An i.v. injection of USPIO particles increases R_2* in tissue surrounding blood vessels that are perfused with blood plasma at the time of injection. With a known blood concentration of USPIO particles, $\Delta R_2^*_{USPIO}$ can be used to calculate blood volume. Due to the difference in size of erythrocytes and USPIO particles, (~6µm and 0.03µm, respectively [2]), the volume of distribution influenced by hyperoxia and USPIO is likely to differ, with small vessels offering preferential access to USPIO particles. Tumour vascular morphology and function is highly dependent on both tumour size and site of implantation. Furthermore, orthotopically propagated models may more closely mimic human metastatic tumour growth and pathophysiology, resulting in differing vascular characteristics than those found in an equivalent subcutaneous model [3]. **Given that many cancer therapies rely on vascular delivery to the tumour, this level of understanding of tumour vasculature in pre-clinical models is imperative. The aim of this study was to use CUSPIO imaging to investigate vascular behaviour and structure in small and large xenograft models, and an orthotopic model, of PC3 prostate tumours, and compare the differences in these characteristics between the different models.**

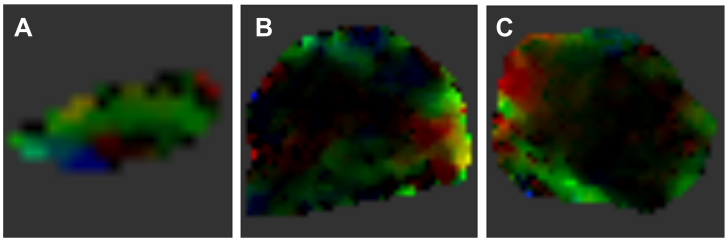

Figure 1. Representative RGB maps showing the spatial distribution of ΔR_2* responses for small (A) and large (B) subcutaneous, and orthotopic (C) tumours derived from a PC3 cell line

Methods: *Data Acquisition:* Male NCr nude mice were injected either subcutaneously on the right flank, or intraprostatically, with 1×10^6 PC3 cells. The subcutaneous cohort was split into two groups of six mice. The tumours from group 1 were imaged a week later at an average tumour diameter of 4.8 ± 0.5mm. The tumours from group 2 were imaged three weeks following inoculation at an average diameter of 12.7 ± 1mm. The tumours from the orthotopic cohort were imaged at 3 weeks at an average diameter of 10 ± 1mm. All images were acquired on a 7T horizontal bore Bruker system using a 3cm birdcage coil. The mice were anesthetised and restrained using dental paste in order to limit motion artefacts [4]. T_2w morphological (turboRARE) images were acquired for tumour delineation, followed by two baseline multi gradient echo MGE acquisitions (3 contiguous 1mm slices, TR=200msec, TE=6–28ms, 4ms echo spacing, 8 averages) acquired during air breathing. The supply was then switched to carbogen, delivered via a nosepiece. Following a two minute transition time, a further identical MGE image set was acquired. The gas supply was then reverted to air and, after a 10 minute transition time to clear residual carbogen, a second baseline MGE image set was acquired. A final MGE image set was acquired one minute after injection of 200µmol/kg USPIO (ferumoxtran-10, Sinerem, Guerbet) via a cannulated tail vein. *Data Analysis:* Using a previously described method, MGE data were fitted using a Bayesian approach which took into account the Rician data distribution [5]. This method enabled calculation of the probability that a given estimate of ΔR_2* in each pixel was significantly greater than zero. This allows the exclusion of voxels where there was non-significant change in R_2*. RGB maps were generated with a red channel designated to pixels with a positive $\Delta R_2^*_{carbo}$, the blue channel to pixels with negative $\Delta R_2^*_{carbo}$ and the green channel to positive $\Delta R_2^*_{USPIO}$. Regions with both negative $\Delta R_2^*_{carbo}$ and positive $\Delta R_2^*_{USPIO}$ therefore appeared cyan (blue + green) and regions with both positive $\Delta R_2^*_{carbo}$ and positive $\Delta R_2^*_{USPIO}$ appeared yellow (red + green).

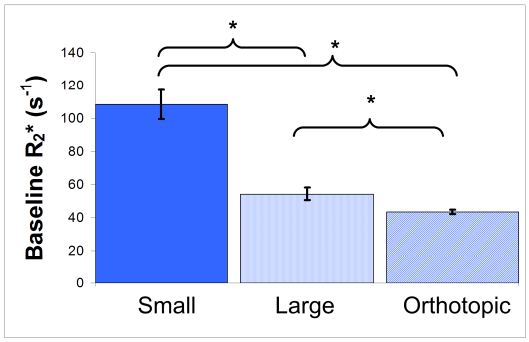

Figure 2. Median baseline R_2* values for small and large subcutaneous, and orthotopic PC3 prostate tumours ($p<0.05$)

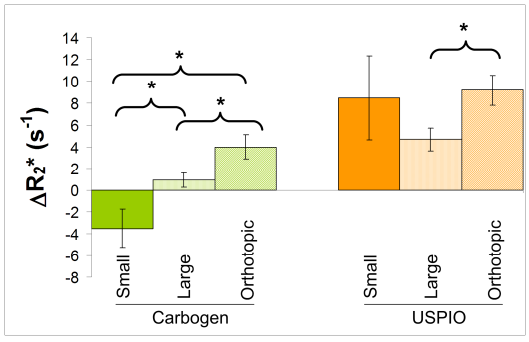

Figure 3. Median $\Delta R_2^*_{carbogen}$ and $\Delta R_2^*_{USPIO}$ values for small and large subcutaneous, and orthotopic PC3 prostate tumours ($p<0.05$)

Results and Discussion: The median values of baseline R_2*, $\Delta R_2^*_{carbogen}$ and $\Delta R_2^*_{USPIO}$, for each tumour cohort are reported in Figures 2 and 3 respectively. Small, large and orthotopic tumour cohorts all exhibited significantly different median baseline R_2*, and $\Delta R_2^*_{carbogen}$. Median $\Delta R_2^*_{USPIO}$ was only significantly different for the large and orthotopic tumour cohorts (figure 2). The significant difference in $\Delta R_2^*_{carbogen}$ exhibited by the three tumour cohorts suggests differences in the haemodynamic functionality of the vasculature in each cohort. Furthermore, the negative median $\Delta R_2^*_{carbogen}$ seen in the small tumour cohort suggests that the small tumours were characterised by functional, erythrocyte perfused, vasculature. The positive median $\Delta R_2^*_{carbogen}$ seen in both the large and orthotopic tumour cohorts is consistent with vascular steal. The significantly different $\Delta R_2^*_{USPIO}$ in the large subcutaneous and orthotopic PC3 tumours suggests a difference in blood volume which was backed up by Hoescht 33342 histology (data not shown).

Representative CUSPIO RGB maps for small, large and orthotopic PC3 tumours are shown in Figure 1. RGB maps for all tumours show regions, as seen in previous data, where there is significant $\Delta R_2^*_{carbogen}$, but no significant $\Delta R_2^*_{USPIO}$. This data suggests these regions have experienced a vascular shutdown in the period between the carbogen breathing and the USPIO particle injection. RGB maps from all tumour cohorts also show a heterogeneous distribution of $\Delta R_2^*_{USPIO}$, which is indicative of heterogeneous perfusion in the tumour model. This may have consequences for the delivery of therapeutic molecules that are of the same order of size as a USPIO particle. There was no significant difference in the spatial distribution of CUSPIO ΔR_2* response categories between the three tumour cohorts.

Conclusions: Significant differences were measured in both baseline R_2*, and ΔR_2* during carbogen breathing in small and large subcutaneous, and orthotopic PC3 tumours, which are thought to reflect differences in the vascular structure and behaviour of tumours grown from the same cell line but of different sizes and in different sites. A significant difference in ΔR_2* after USPIO injection was also seen in the large subcutaneous and orthotopic PC3 tumours, suggesting a difference in blood volume. These results have important implications in the understanding of drug delivery to tumours and how this information is translated from pre-clinical rodent models to a clinical situation.

Acknowledgements: This work was supported by BBSRC, AstraZeneca, The Royal Society, Cancer Research UK grant number C1060/A5117 and also NHS funding to the NIHR Biomedical Research Centre. We acknowledge the support received from the CRUK and EPSRC Cancer Imaging Centre in association with the MRC and Department of Health (England) grant C1060/A10334, also NHS funding to the NIHR Biomedical Research Centre

References:

1.Burrell, J. ISMRM, 2009. 2.Jung, C.W. and P. Jacobs, Mag Res Imaging, 1995. 13(5) 3.Denekamp, J. NMR Biomed, 1992. 5(5): 4.Landuyt, W., et al. J Mag Res Imaging, 2002. 16(2): 5.Walker-Samuel, S. in *ISMRM Cancer Workshop, Nice*. 2008. 6.Tropres, I., et al. Magn Reson Med, 2001. 45(3):